catalysts

MDPI

Article

Extended Hydrogen-Bonded Molybdenum Arrays Derived from Carboxylic Acids and Dianilines: ROP Capability of the Complexes and Parent Acids and Dianilines

William Clegg [1], Mark R. J. Elsegood [2] and Carl Redshaw [3,*]

[1] Chemistry, School of Natural and Environmental Sciences, Newcastle University, Newcastle upon Tyne NE1 7RU, UK; bill.clegg@ncl.ac.uk
[2] Chemistry Department, Loughborough University, Loughborough LE11 3TU, UK; m.r.j.elsegood@lboro.ac.uk
[3] Plastics Collaboratory, Chemistry, School of Natural Sciences, University of Hull, Hull HU6 7RX, UK
* Correspondence: c.redshaw@hull.ac.uk

Abstract: From reactions involving sodium molybdate and dianilines [2,2′-$(NH_2)C_6H_4]_2(CH_2)_n$ (n = 0, 1, 2) and amino-functionalized carboxylic acids 1,2-$(NH_2)(CO_2H)C_6H_4$ or 2-$H_2NC_6H_3$-1,4-$(CO_2H)_2$, in the presence of Et_3N and Me_3SiCl, products adopting H-bonded networks have been characterized. In particular, the reaction of 2,2′-diaminobiphenyl, [2,2′-$NH_2(C_6H_4)]_2$, and 2-aminoterephthalic acid, $H_2NC_6H_3$-1,4-$(CO_2H)_2$, led to the isolation of [$(MoCl_3$[2,2′-$N(C_6H_4)]_2$}{HNC_6H_3-1-(CO_2),4-(CO_2H)]·2[2,2′-$NH_2(C_6H_4)]_2$·3.5MeCN (**1**·3.5MeCN), which contains intra-molecular N–H···Cl H-bonds and slipped π···π interactions. Similar use of 2,2′-methylenedianiline, [2,2′-$(NH_2)C_6H_4]_2CH_2$, in combination with 2-aminoterephthalic acid led to the isolation of [$MoCl_2(O_2CC_6H_3NHCO_2SiMe_3)$ $(NC_6H_4CH_2C_6H_4NH_2)$]·3MeCN(**2**·3MeCN). Complex **2** contains extensive H-bonds between pairs of centrosymmetrically-related molecules. In the case of 2,2′ethylenedianiline, [2,2′-$(NH_2)C_6H_4]_2CH_2CH_2$, and anthranilic acid, 1,2-$(NH_2)(CO_2H)C_6H_4$, reaction with Na_2MoO_4 in the presence of Et_3N and Me_3SiCl in refluxing 1,2-dimethoxyethane afforded the complex [$MoCl_3${1,2-(NH)$(CO_2)C_6H_4$}{NC_6H_4 $CH_2CH_2C_6H_4NH_3$}]·MeCN (**3**·MeCN). In **3**, there are intra-molecular bifurcated H-bonds between NH_3 H atoms and chlorides, whilst pairs of molecules H-bond further via the NH_3 groups to the non-coordinated carboxylate oxygen, resulting in H-bonded chains. Complexes **1** to **3** have been screened for the ring opening polymerization (ROP) of both ε-caprolactone (ε-CL) and δ-valerolactone (δ-VL) using solvent-free conditions under N_2 and air. The products were of moderate to high molecular weight, with wide Đ values, and comprised several types of polymer families, including OH-terminated, OBn-terminated (for PCL only), and cyclic polymers. The results of metal-free ROP using the dianilines [2,2′-$(NH_2)C_6H_4]_2(CH_2)_n$ (n = 0, 1, 2) and the amino-functionalized carboxylic acids 1,2-$(NH_2)(CO_2H)C_6H_4$ or 2-$H_2NC_6H_3$-1,4-$(CO_2H)_2$ under similar conditions (no BnOH) are also reported. The dianilines were found to be capable of the ROP of δ-VL (but not ε-CL), whilst anthranilic acid outperformed 2-aminoterephthalic acid for both ε-Cl and δ-VL.

Keywords: hydrogen-bonded network; amino-functionalized carboxylic acids; dianilines; molybdenum complexes; solid-state structures; ring opening polymerization (ROP); metal-free ROP; cyclic esters

Citation: Clegg, W.; Elsegood, M.R.J.; Redshaw, C. Extended Hydrogen-Bonded Molybdenum Arrays Derived from Carboxylic Acids and Dianilines: ROP Capability of the Complexes and Parent Acids and Dianilines. *Catalysts* **2024**, *14*, 214. https://doi.org/10.3390/catal14030214

Academic Editor: Mauro Bassetti

Received: 23 January 2024
Revised: 13 March 2024
Accepted: 15 March 2024
Published: 21 March 2024

1. Introduction

Despite the intensive research on imido compounds over the last few decades, driven partly by their presence in metathesis catalysts [1], examples of complexes bearing highly functionalized imido ligation remain somewhat limited [2]. With this in mind, we have been interested in exploiting amino-functionalized carboxylic acids, and our early work focused on the use of anthranilic acid [3–5], and in separate studies we have reported the use of potentially chelating dianilines, to access new structural motifs [6,7]. Our entry into such chemistry is via sodium molybdate, which is combined with anilines in the presence of triethylamine and trimethylsilyl chloride, using refluxing dimethoxyethane

as the solvent [8–11]. The use of dianilines or amino-functionalized carboxylic acids in combination with molybdate under such conditions has the potential to afford products with extensive intra- and/or inter-molecular hydrogen bonding. For example, use of $[(2\text{-}NH_2C_6H_4)_2O]$ led to the salt $[Et_3NH][MoCl_4[(2\text{-}NH_2C_6H_4)(2\text{-}NC_6H_4)O]$ comprising discrete units of two anions and two cations linked by a series of H-bonds [11]. We also note that chiral diimido complexes (of Mo and W) have been reported by Sundermeyer et al. [12]. Herein, we combine the two sets of 'ligands' in one pot, i.e., an amino-functionalized carboxylic acid and a chelating dianiline, with the aim of further increasing the degree of hydrogen bonding present. In particular, use of the dianilines $[2,2'\text{-}(NH_2)C_6H_4]_2(CH_2)_n$ (n = 0, 1, 2), in combination with either anthranilic acid or 2-aminoterephthalic acid, in the 'molybdate' preparation led to products (Scheme 1) with extensive intra- and inter-molecular interactions resulting in the formation of H-bonded pairs, chains, or a 3D network.

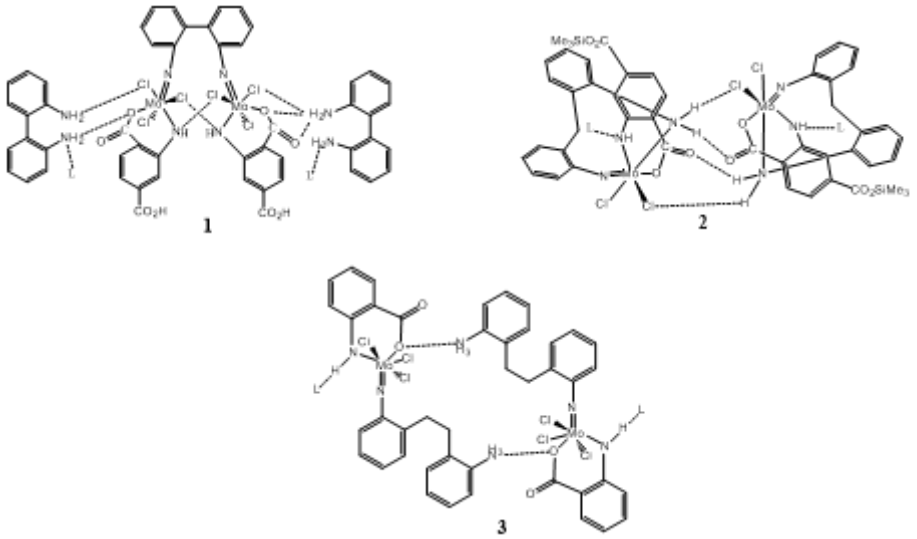

Scheme 1. Complexes **1**–**3** isolated in this work (L = MeCN).

Given the interest in alternatives to petroleum-derived plastics [13], there is currently much research devoted to seeking catalysts that are capable of producing greener polymers via ring opening polymerization (ROP) of cyclic esters. Both transition metal and metal-free ROP systems are attracting interest [14–24]. Ideally, such catalysts should be highly active, inexpensive, and non-toxic. In the case of metals, the use of earth-abundant metals is now attracting attention [25]. In terms of molybdenum-based systems, the limited number that have thus far been reported tend to exhibit activity only at elevated temperatures, with early examples based on ammonium decamolybdate (melt at 150 °C) [26] or bis-(salicylaldhydato)dioxomolybdenum (110 °C in mesitylene) [27]. More recent examples include oxo and imido complexes derived from chelating phenols [28,29], or the oxydianiline $[(2\text{-}NH_2C_6H_4)_2O]$ [11], or a family of iodoanilines [30]. For many of these molybdenum-based systems, trans-esterification is evident. Given the somewhat limited arsenal of molybdenum-based ROP catalysts, we have investigated the three complexes herein (shown in Scheme 1) for their potential in the ROP of ε-caprolactone and δ-valerolactone. Moreover, given the aforementioned interest in metal-free catalysts for ROP, we have also examined the use of the precursor anilines and acids (Scheme 2) employed in the synthesis of **1**–**3** as ROP catalysts. We also note that there is growing interest in the ability of hydrogen bonding to promote ROP, particularly in carboxylic acid-based systems [31] and amine/amide-containing systems [32–39].

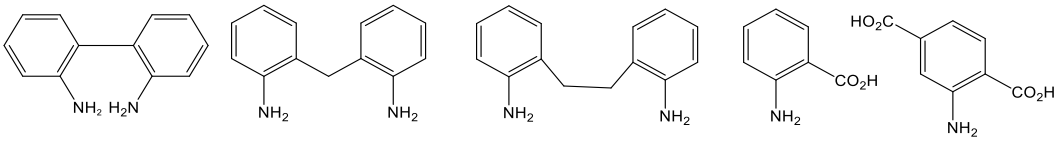

Scheme 2. Dianilines and acids employed herein.

2. Results and Discussion

2.1. Synthesis and Characterization of Hydrogen-Bonded 2,2′-Diaminobiphenyl-Derived Molybdenum Complex

Use of the established sodium molybdate/aniline/Et_3N/Me_3SiCl preparation [8–11] but employing a combination of 2,2′-diaminobiphenyl [2,2′-$NH_2(C_6H_4)]_2$ and 2-aminoterephthalic acid $H_2NC_6H_3$-1,4-$(CO_2H)_2$ as the amine sources, following work-up (MeCN), led to the isolation of small orange/red prisms in moderate yield. In the IR spectrum, a broad peak at 3444 cm^{-1} is assigned to *v*NH (Figure S1, SI). Single crystals suitable for X-ray diffraction were obtained from a saturated acetonitrile solution at 0 °C. The molecular structure is shown in Figure 1, with selected bond lengths and angles given in the caption; alternative views are given in Figure S2, SI. The asymmetric unit comprises one molybdenum-containing complex, two 2,2′-diaminobiphenyl molecules, and three and a half acetonitrile solvent molecules of crystallization, i.e., [($MoCl_3$[2,2′-$N(C_6H_4)]_2$}{HNC_6H_3-1-(CO_2),4-(CO_2H)]·2[2,2′-$NH_2(C_6H_4)]_2$·3.5MeCN **1**·2[2,2′-$NH_2(C_6H_4)]_2$·3.5MeCN. The metal complex ligand conformations are supported by intra-molecular N–H···Cl H-bonds (Table 1) and the two amino-terephthalate ligands adopt a slipped π···π interaction with C(16) and C(23) overlaying the centroid of the aromatic ring of the opposite ligand at a distance of ca. 3.5 Å. The closest atom···atom contacts are: C(15)···C(22) = 3.334 Å; C(20)···C(26) = 3.487 Å; and C(17)···C(24) = 3.535 Å. Thus, the rings are closer at the N end.

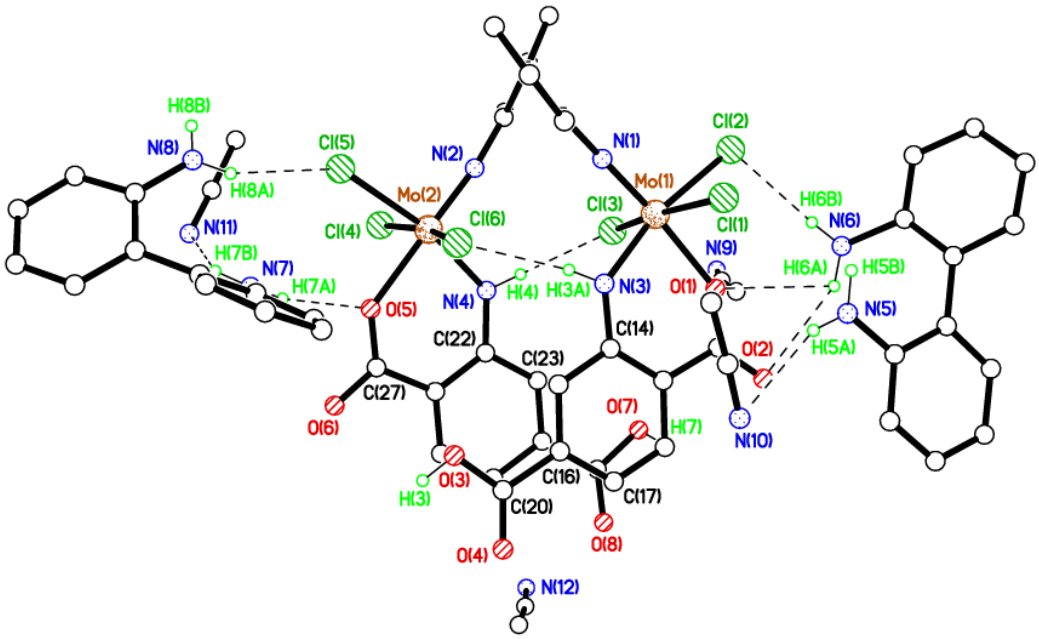

Figure 1. Molecular structure of **1**·2[2,2′-$NH_2(C_6H_4)]_2$·3.5MeCN. Selected bond lengths (Å) and angles (°): Mo(1)–N(1) 1.715(9), Mo(1)–N(3) 1.977(8), Mo(1)–O(1) 2.092(6), Mo(1)–Cl(1) 2.386(3), Mo(1)–Cl(2) 2.455(2), Mo(1)–Cl(3) 2.421(2); O(1)–Mo(1)–N(3) 81.7(3), Cl(2)–Mo(1)–N(3) 167.5(2), N(1)–Mo(1)–O(1) 170.9(3). Elements are shown in different representations (C black, H pale green, N blue, O red, Cl green, Mo brown) and hydrogen bonds are shown as dashed lines (in all structural figures).

Table 1. Hydrogen-bond geometry (Å, °) for **1**·2[2,2′-$NH_2(C_6H_4)$]$_2$·3.5MeCN.

D—H···*A*	*D*—H	H···*A*	*D*···*A*	*D*—H···*A*
N3—H3*A*···Cl6	0.88	2.42	3.278 (8)	164
O3—H3···O2 [i]	0.84	1.73	2.564 (9)	170
N4—H4···Cl3	0.88	2.32	3.190 (8)	172
O7—H7···O6 [ii]	0.84	1.89	2.707 (10)	165
N5—H5*A*···N10	0.88	2.53	3.37 (2)	159
N5—H5*B*···Cl4 [iii]	0.88	2.74	3.413 (11)	135
N6—H6*A*···O2	0.88	2.56	3.319 (12)	145
N6—H6*A*···N5	0.88	2.28	2.736 (13)	112
N6—H6*B*···Cl2	0.88	2.44	3.307 (9)	170
N7—H7*A*···O5	0.88	2.13	2.990 (10)	165
N7—H7*B*···N11	0.88	2.34	3.02 (2)	135
N8—H8*A*···Cl5	0.88	2.95	3.432 (11)	116

Symmetry codes: (i) $x + 1/2, -y + 3/2, z + 1/2$; (ii) $x - 1/2, -y + 3/2, z - 1/2$; (iii) $x - 1, y, z$.

The Mo_2 complex is capped at each end with a neutral, co-crystallized $C_{12}H_{12}N_2$ molecule via 2 or 3 N–H···Cl or N–H···O H-bonds. The NH_2 H atoms also H-bond to MeCN molecules of crystallization or symmetry-related Mo_2 complexes. The carboxylic acid OH groups H-bond to the carboxylate oxygen atoms of neighboring Mo_2 complexes via charge-assisted H-bonds, so they do not form the often-observed carboxylic acid head-to-tail $R^2_2(8)$ motif (Figure 2) [40,41].

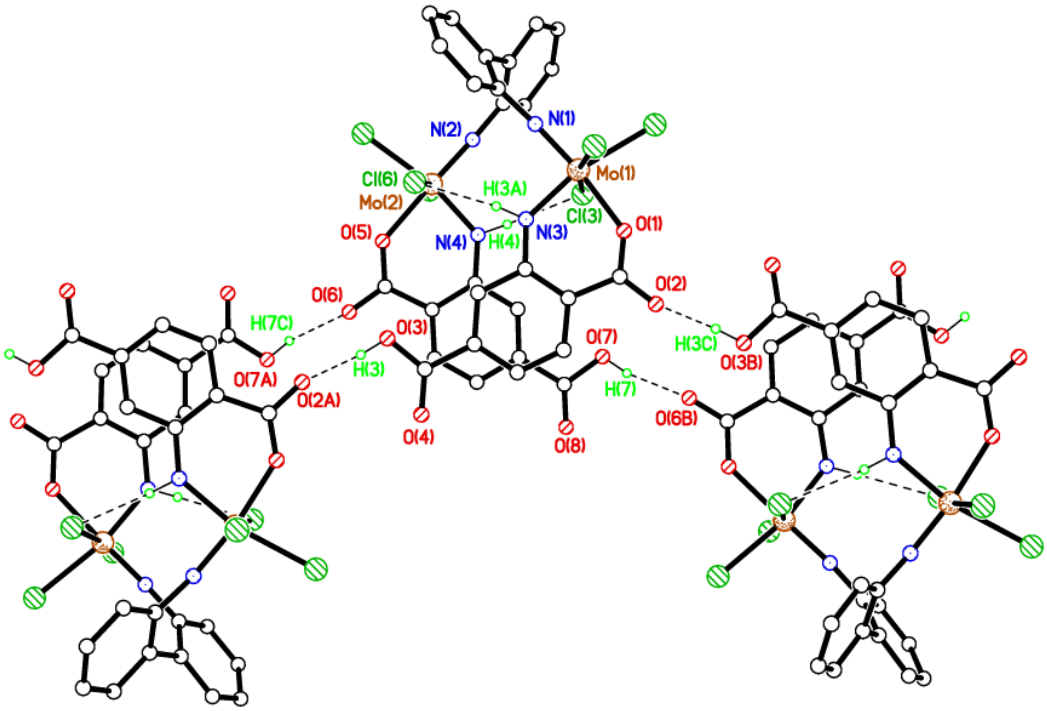

Figure 2. View of H-bonded chains running parallel to *c*.

The only NH hydrogen atom that does not act as an H-bond donor is H(8B), presumably due to the lack of a suitably positioned acceptor. The structure adopts a 3D H-bonded network overall (Figure 3).

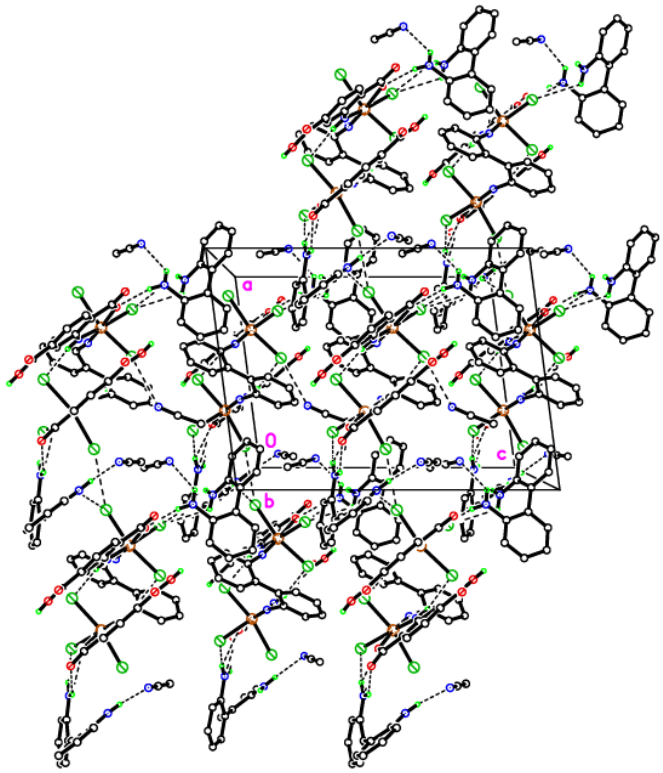

Figure 3. H-bonded 3D network of **1**·2[2,2′-$NH_2(C_6H_4)]_2$·3.5MeCN.

The MALDI-ToF spectrum of **1**·2[2,2′-$NH_2(C_6H_4)]_2$·3.5MeCN is given in Figure S3, SI; for assignments see experimental Section 4.1. Complex **1** (and **2** and **3** below) despite being recrystallized from MeCN proved to be insoluble in common organic solvents, which not only hampered characterization in solution (e.g., only a weak ^{1}H NMR spectrum of **1** was obtained, Figure S4, SI for the aromatic region), but also restricted our ROP studies to the melt phase, vide infra.

2.2. Synthesis and Characterization of the Methylene-Bridged Dianiline-Derived Molybdenum Complex

We then investigated the use of the methylene-bridged dianiline [2,2′-$(NH_2)C_6H_4]_2CH_2$ in combination with 2-aminoterephthalic acid $H_2NC_6H_3$-1,4-$(CO_2H)_2$. Following work-up (extraction into MeCN), orange crystals were isolated, which were subjected to a single-crystal X-ray determination. The molecular structure is shown in Figure 4, with selected bond lengths and angles given in the caption. The asymmetric unit comprises one molybdenum complex and three molecules of non-coordinated acetonitrile. The dianiline-derived ligand binds in imido/amine fashion about the octahedral metal center, whilst the 2-aminoterephthalic acid binds in carboxylate/amide fashion. In the IR spectrum (Figure S5, SI), there are peaks at 3501, 3446, and 3385 cm^{-1}, which are assigned to *ν*NH. Interestingly, a trimethylsilylation has occurred at the 2-aminoterephthalic acid, as has been observed previously in the system $[Et_3NH][MoCl_3\{2\text{-}(HN)C_6H_4CO_2\}\{2\text{-}Me_3SiO_2CC_6H_4N\}]$ [2]. Moreover, a search of the Cambridge Structural Database (CSD) reveals four other occurrences of this type of $PhCO_2SiMe_3$ motif [42–45]. The coordination around molybdenum is completed by two chloride ligands, which are trans to the amine and amide functions. The formula can thus be written as $[MoCl_2(O_2CC_6H_3NHCO_2SiMe_3)(NC_6H_4CH_2C_6H_4NH_2)]$·3MeCN (**2**·3MeCN).

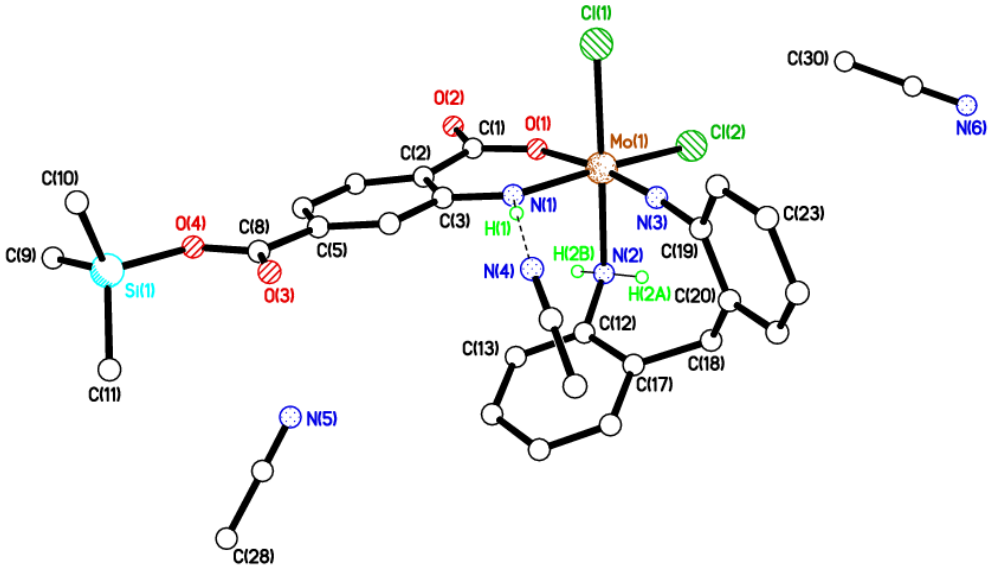

Figure 4. Molecular structure of $[MoCl_2(O_2CC_6H_3NHCO_2SiMe_3)(NC_6H_4CH_2C_6H_4NH_2)]\cdot 3MeCN$ (**2**·3MeCN). Selected bond lengths (Å) and angles (°): Mo(1)–O(1) 2.0644(9), Mo(1)–N(1) 1.9428(11), Mo(1)–N(2) 2.2375(11), Mo(1)–N(3) 1.7370(11), Mo(1)–Cl(1) 2.3643(3), Mo(1)–Cl(2) 2.4267(3); N(1)–Mo(1)–O(1) 82.81(4), N(2)–Mo(1)–N(3) 90.85(4).

Pairs of centrosymmetrically-related molecules are connected via H-bonds utilizing both NH_2 hydrogen atoms as donors and a chloride and non-coordinated carboxylate oxygen as acceptors (Figure 5 and Table 2); alternative views are given in Figure S6, SI. The angle between the two aromatic rings in the imido ligand is 75.99 (4)°. The N–H group forms an H-bond to one of the three molecules of crystallization. The MALDI-ToF spectrum of $[MoCl_2(O_2CC_6H_3NHCO_2SiMe_3)(NC_6H_4CH_2C_6H_4NH_2)]\cdot 3MeCN$ (**2**·3MeCN) is given in Figure S7, SI; for assignments see experimental Section 4.2.

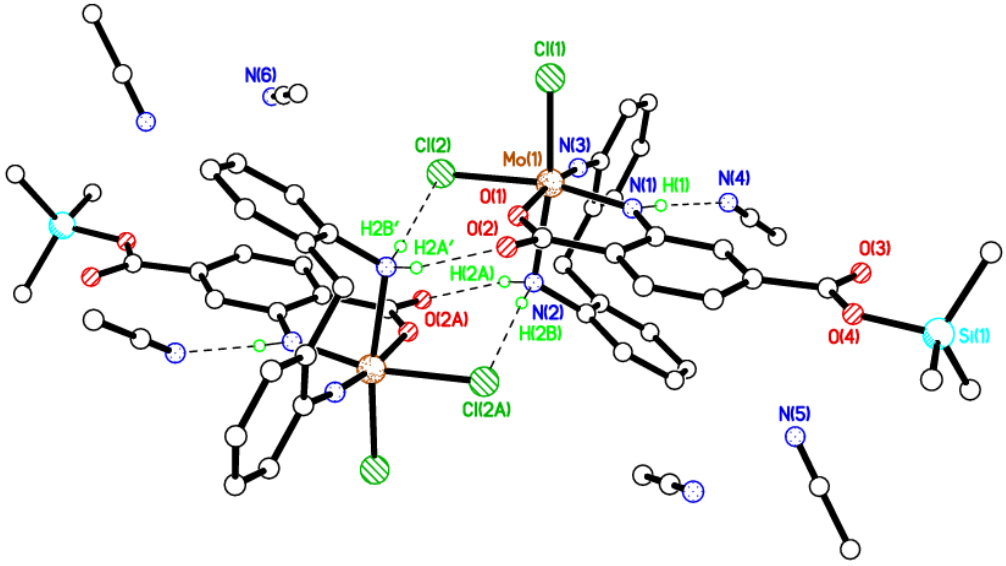

Figure 5. H-bonds between pairs of centrosymmetrically-related molecules in **2**·3MeCN.

Table 2. Hydrogen-bond geometry (Å, °) for **2**·3MeCN.

D—H···*A*	*D*—H	H···*A*	*D*···*A*	*D*—H···*A*
N1—H1···N4	0.82 (1)	2.13 (1)	2.9518 (17)	176 (2)
N2—H2*A*···O1 [i]	0.81 (1)	2.47 (2)	2.9215 (14)	116 (2)
N2—H2*A*···O2 [i]	0.81 (1)	2.28 (1)	3.0736 (15)	168 (2)
N2—H2*B*···Cl2 [i]	0.84 (1)	2.68 (1)	3.5139 (11)	174 (2)

Symmetry codes: (i) $-x+1, -y, -z+1$.

2.3. Synthesis and Characterization of the Ethylene-Bridged Dianiline-Derived Molybdenum Complex

The length of the bridge in the dianiline was then extended to an ethylene linkage, namely [2,2′-$(NH_2)C_6H_4]_2CH_2CH_2$, and, to avoid the previous silylation issue, anthranilic acid 1,2-$(NH_2)(CO_2H)C_6H_4$ was employed rather than 2-aminoterephthalic acid. Work-up as before led to the isolation of purple crystals of X-ray diffraction quality. In the IR spectrum (Figure S8, SI), there are peaks at 3452/3348 cm^{-1}, which are assigned to *ν*NH. The molecular structure is shown in Figure 6, with selected bond lengths and angles given in the caption; alternative views are given in Figure S9, SI. This purple complex was identified as [$MoCl_3${1,2-$(NH)(CO_2)C_6H_4$}{$NC_6H_4CH_2CH_2C_6H_4NH_3$}]·MeCN (**3**·MeCN) and formed in good yield (*ca*. 65%). Single crystals suitable for X-ray diffraction were obtained from a saturated acetonitrile solution at 0 °C. In the asymmetric unit, there are two independent Mo complexes and two MeCN molecules of crystallization. The two molybdenum-containing zwitterionic molecules differ slightly in their conformations in the solid state. For example, the two rings in the N—N groups are twisted relative to each other by different amounts: C(8) > C(13) vs. C(16) > C(21) = 49.81 (13)° and C(29) > C(34) vs. C(37) > C(42) = 30.87 (13)°. In both unique complexes, there are intra-molecular bifurcated H-bonds between one of the NH_3 H atoms and the coordinated chlorides Cl(1) and Cl(2) or Cl(5) and Cl(6). The two MeCN solvent molecules of crystallization both act as H-bond acceptors from the N–H groups at N(1) and N(4) (Table 3).

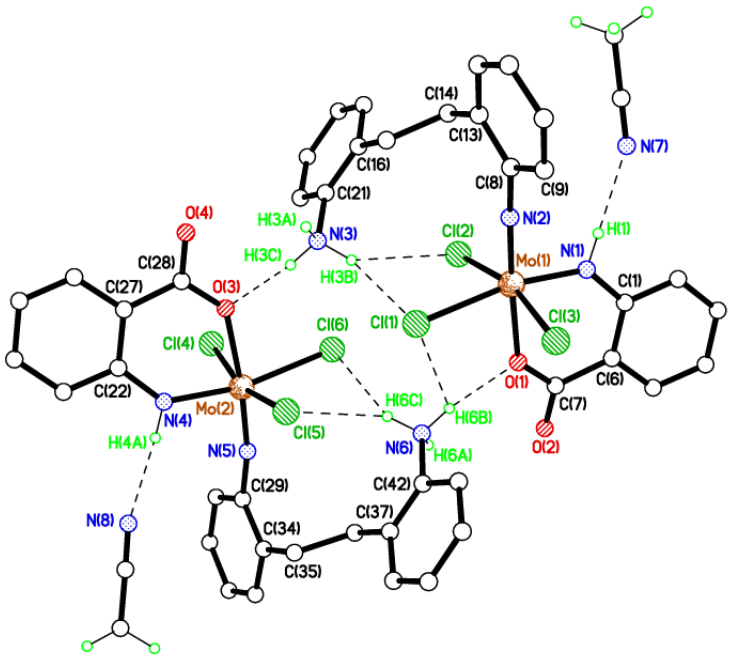

Figure 6. Molecular structure of **3**·MeCN. Selected bond lengths (Å) and angles (°): Mo(1)–N(1) 1.939(3), Mo(1)–N(2) 1.730(2), Mo(1)–O(1) 2.1137(19), Mo(1)–Cl(1) 2.4535(8), Mo(1)–Cl(2) 2.3963(8), Mo(1)–Cl(3) 2.4071(9); N(1)–Mo(1)–O(1) 82.72(9), O(1)–Mo(1)–N(2) 177.09(10).

Table 3. Hydrogen-bond geometry (Å, °) for **3**·MeCN.

D—H···*A*	*D*—H	H···*A*	*D*···*A*	*D*—H···*A*
N1—H1···N7	0.81 (2)	2.19 (2)	2.995 (4)	172 (3)
N3—H3*A*···O2 [i]	0.87 (2)	1.96 (2)	2.828 (3)	172 (3)
N3—H3*B*···Cl1	0.87 (2)	2.54 (2)	3.323 (3)	151 (3)
N3—H3*B*···Cl2	0.87 (2)	2.85 (3)	3.502 (3)	133 (3)
N3—H3C···O3	0.88 (2)	1.93 (2)	2.803 (3)	174 (3)
N3—H3C···O4	0.88 (2)	2.55 (3)	3.054 (3)	117 (2)
N4—H4···N8	0.81 (2)	2.21 (2)	3.010 (4)	170 (3)
N6—H6*A*···O4 [ii]	0.88 (2)	1.98 (2)	2.847 (3)	171 (3)
N6—H6*B*···Cl1	0.87 (2)	2.99 (3)	3.446 (3)	115 (2)
N6—H6*B*···O1	0.87 (2)	2.00 (2)	2.858 (3)	171 (3)
N6—H6*B*···O2	0.87 (2)	2.59 (3)	3.059 (3)	115 (2)
N6—H6C···Cl5	0.87 (2)	2.70 (2)	3.416 (3)	141 (3)
N6—H6C···Cl6	0.87 (2)	2.59 (2)	3.326 (3)	143 (3)

Symmetry codes: (i) $x, -y + 1/2, z + 1/2$; (ii) $x, -y + 1/2, z - 1/2$.

In the packing of **3**·MeCN, the two unique Mo complexes H-bond in a head-to-tail fashion via the NH_3 groups to a coordinated carboxylate oxygen atom in the case of H(3C) to O(3), or via a bifurcated pair of interactions between H(6B) and O(1) and Cl(1); this is not over a crystallographic inversion center. These pairs of molecules then H-bond further to other molecules via the NH_3 groups to the non-coordinated carboxylate, resulting in H-bonded chains running parallel to *c* (Figure 7). These diamond-shaped interactions again occur in head-to-tail pairs not dictated by crystallographic inversion symmetry, involving O(2) and O(4).

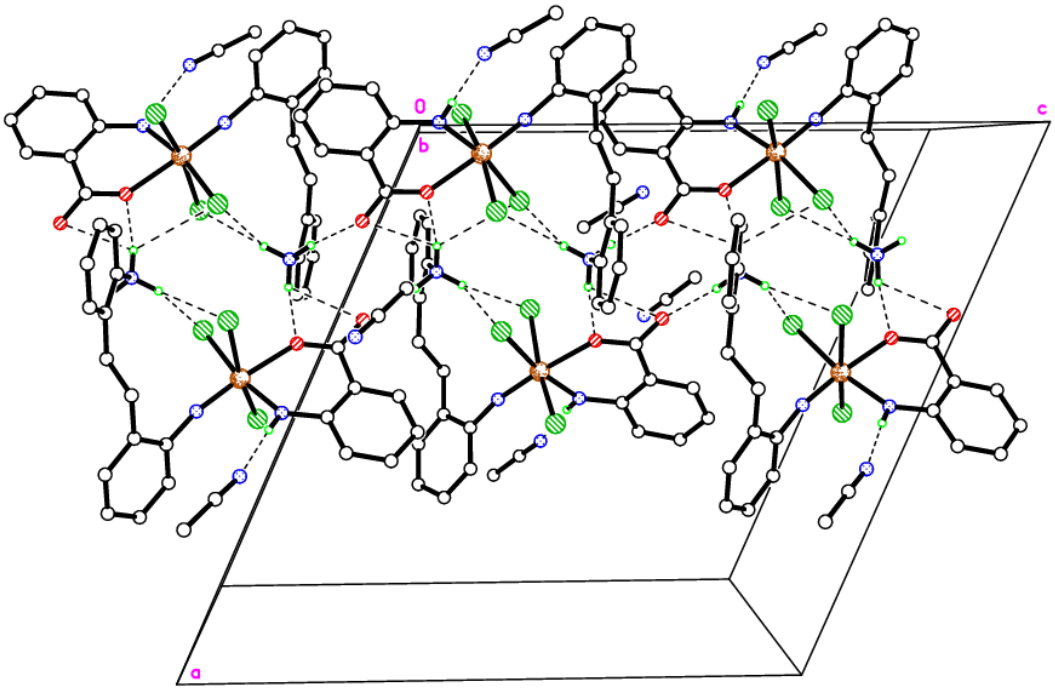

Figure 7. View of H-bonded chains running parallel to *c* for **3**·MeCN.

The MALDI-ToF spectrum of $[MoCl_3\{1,2\text{-}(NH)(CO_2)C_6H_4\}\{NC_6H_4CH_2CH_2C_6H_4NH_3\}]\cdot$MeCN (**3**·MeCN) is given in Figure S10, SI; for assignments see experimental Section 4.3.

3. Ring Opening Polymerization (ROP)

3.1. Ring Opening Polymerization of ε-Caprolactone (ε-CL)

Complexes **1**–**3** have been screened for their ability to act as catalysts in the presence of benzyl alcohol (BnOH) for the ROP of ε-caprolactone, and the results are presented in

Table 4. Results for **1**–**3** are compared with the related molybdenum-containing complexes **I** and **II** [11] (see Figure 8). Based on previous molybdenum ROP studies in our group [11,28–30], we selected the conditions of 130 °C with a ratio of ε-CL to complex of 500:1 in the presence of one (for **2** and **3**) or two (for **1**) equivalents of benzyl alcohol per metal over 24 h, i.e., a [CL]:[catalyst]:[BnOH] ratio of 500:1:1 or 500:1:2. However, given the aforementioned problematic issues with solubility, the complexes herein were only screened as melts under either N_2 or air (see Table 4). All complexes were found to be active under these polymerization conditions with similar monomer conversions (>95%, e.g., Figures S11–S14, SI), affording relatively high molecular weight polymers, with **3** under N_2 (Entry 5, Table 4) affording the highest at ca. 31,650 Da, albeit with poor control (Đ = 3.66); selected gpc traces are given in Figures S15–S21. End group analysis by ^{1}H NMR spectroscopy reveals signals at 3.63, 5.09, and 7.34 ppm consistent with the presence of a BnO end group, which indicates that the polymerization proceeds through a coordination-insertion mechanism, whereby the monomer coordinates to the metal followed by the acyl oxygen bond cleavage of the monomer and chain propagation. Interestingly, consistent with the wide Đ values, the MALDI-TOF spectra revealed several families of products including OH terminated polymers, OBn terminated polymers, and cyclic polymers (e.g., Figures 9 and 10; expansions are given in the SI, Figures S22–S25). There was evidence of trans-esterification, and all observed M_n values were significantly lower than the calculated values.

Table 4. The ROP of ε-CL catalyzed by **1**–**3** and **I, II**.

Entry	Catalyst	[CL]:[Cat]:BnOH	Conversion [a] (%) [b]	M_n *(obsd)* [b]	M_n Corrected [c]	M_n*calc* [d]	Đ [b]
1	**1**	500:1:2	100	14,820	8300	57,180	2.78
2 [e]	**1**	500:1:2	100	16,590	9290	57,180	3.00 3.00
3	**2**	500:1:1	100	10,430	5840	57,180	1.12
4 [e]	**2**	500:1:1	99	22,880	12,810	56,610	1.85
5	**3**	500:1:1	86	56,520	31,650	49,190	3.66
6 [e]	**3**	500:1:1	99	34,200	19,150	56,610	2.84
7	**I**	500:1:1	100	64,160	35,930	57,180	3.83
8 [e]	**I**	500:1:1	100	34,110	19,100	57,180	3.61
9	**II**	500:1:1	100	21,040	11,780	57,180	2.26
10 [e]	**II**	500:1:1	97	15,620	8750	55,460	3.69
11 [e]	[2,2′-$NH_2(C_6H_4)$]$_2$	500:1	-		-	-	-
12 [e]	[2,2′-$(NH_2)C_6H_4$]$_2CH_2$	500:1	-		-	-	-
13 [e]	[2,2′-$(NH_2)C_6H_4$]$_2CH_2CH_2$	500:1	-		-	-	-
14 [e]	1,2-$(NH_2)(CO_2H)C_6H_4$	500:1	98	14,090	7890	56,070	1.37
15 [e]	$H_2NC_6H_3$-1,4-$(CO_2H)_2$	500:1	28		-	-	-

[a] Determined by ^{1}H NMR spectroscopy; [b] Measured by GPC in THF relative to polystyrene standards; [c] M_n calculated after Mark–Houwink correction [44,45]; M_n corrected = 0.56 × M_n obsd; [d] Calculated from ([monomer]$_0$/[cat]$_0$) × conv (%) × monomer molecular weight (M_{CL} = 114.14) + end groups (OBn/OH used in this case); [e] Conducted in air.

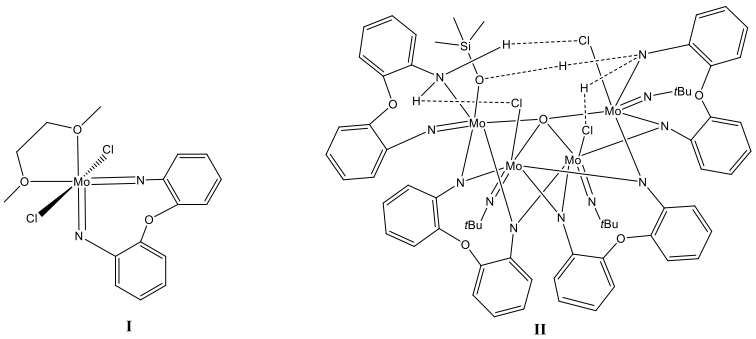

Figure 8. Known complexes **I** and **II**.

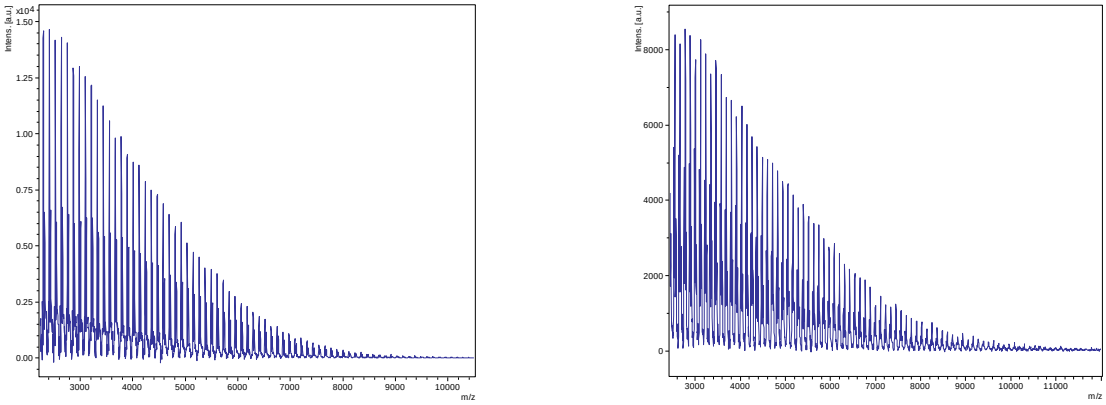

Figure 9. MALDI-ToF spectrum of PCL using **1** left: (Entry 1, Table 4); right (Entry 2, Table 4). For Entry 1, Table 4: The main families are (i) chain polymer (terminated by 2 OH) as sodium adducts [M = 17 (OH) + 1(H) + n × 114.14 (CL) + 22.99 (Na^+)] (e.g., for n = 23, calc. 2666.2 obsv. 2668.4; n = 25 calc. 2894.5 obsv. 2895.9 with peaks offset by about 1.2 Da; (ii) with BnO end groups [M = n × 114.14 (CL) + 108.05 (BnOH) + 22.99 (Na^+)] (e.g., for n = 50 calc. 5838, obsv. 5836.4; for n = 55, calc. 6408.7 obsv. 6406.9) with peaks offset by about 1.7 Da; (iii) cyclic polymers as the potassium adducts, e.g., n = 50 calc. 5746.1 obsv. 5745.7. For Entry 2, Table 4: The main families are (i) chain polymer (terminated by 2 OH) as sodium adducts [M = 17 (OH) + 1(H) + n × 114.14 (CL) + 22.99 (Na^+)], e.g., for n = 30, calc. 3465.2 obsv. 3465.6; n = 40 calc. 4606.6 obsv. 4605.2; (ii) cyclic polymers as the potassium adducts, e.g., n = 50 calc. 5746.1 obsv. 5745.7, n = 60 calc. 6887.5 obsv. 6886.4. Expansions of all the peaks highlighted above can be found in SI (Figures S37 and S38).

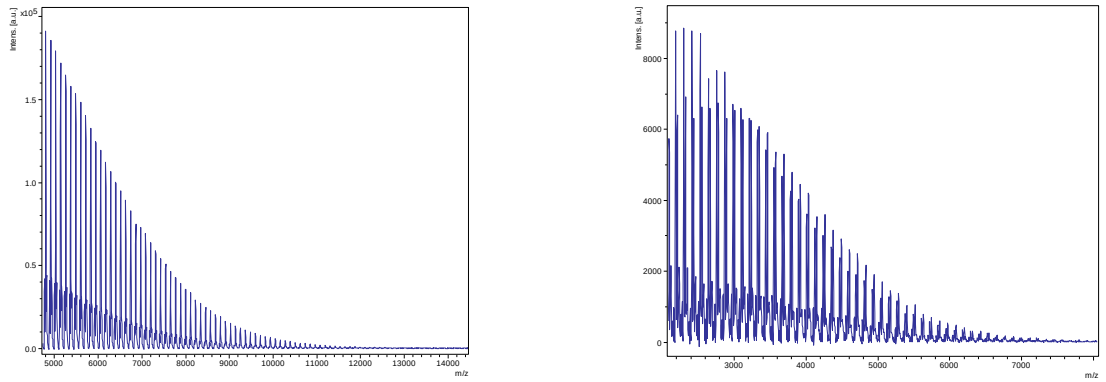

Figure 10. MALDI-ToF spectrum of PCL left using **2** (Entry 3, Table 4); right using **3** (Entry 5, Table 4). For Entry 3, Table 4: The main families are (i) chain polymer (terminated by 2 OH) as sodium adducts [M = 17 (OH) + 1(H) + n × 114.14 (CL) + 22.99 (Na^+)] (e.g., for n = 30, calc. 3465.2 obsv. 3466.3; n = 40 calc. 4606.6 obsv. 4606.2; (ii) cyclic polymers as the potassium adducts e.g., n = 40 calc. 4604.7 obsv. 4606.0; n = 50 calc. 5746.1 obsv. 5747.1. For Entry 5, Table 4: The main family are polymers with BnO end groups as the potassium adducts [M = n × 114.14 (CL) + 108.05 (BnOH) + 39.1 (K^+)] (e.g., for n = 50 calc. 5854.2, obsv. 5854.0). Expansions of all the peaks highlighted above can be found in the SI (Figures S39 and S40).

Given that metal-free catalysts are known [19], the dianilines [2,2′-$(NH_2)C_6H_4]_2(CH_2)_n$ (n = 0, 1, 2) and the amino-functionalized carboxylic acids 1,2-$(NH_2)(CO_2H)C_6H_4$ or 2-$H_2NC_6H_3$-1,4-$(CO_2H)_2$ employed in this work (Scheme 2) to prepare **1**–**3** were screened under similar conditions, albeit in the absence on BnOH for the ROP of ε-CL. In the case of the dianilines, little or no conversion was observed. However, both amino-functionalized carboxylic acids exhibited conversion, with 1,2-$(NH_2)(CO_2H)C_6H_4$ achieving 98%; the MALDI-ToF spectrum (Figure S26, SI) indicated the presence of anthranilic acid-derived

end groups; the ^{1}H NMR spectrum is given in Figure S27, SI. We note that benzoic acid has been shown to be an efficient ROP catalyst for ε-Cl [32].

3.2. Ring Opening Polymerization of δ-Valerolactone (δ-VL)

As in the case of ε-CL, the complexes herein were only screened for the ROP of δ-VL as melts under either N_2 or air (see Table 5) using a ratio of [VL]:[catalyst]:[BnOH] of 500:1:2 (for **1**) or 500:1:1 (for **2**, **3**, and **I**, **II**). All complexes were found to be active under these polymerization conditions with monomer conversions (>75%, Figures S28–S35, SI), affording relatively high molecular weight polymers; selected gpc traces are given in Figures S36–S42, SI. As for CL, the conversions observed for **3** were somewhat lower than for the other systems. The highest molecular weights were afforded by **2** under air (Entry 4, Table 5) and **II** under N_2 (Entry 9, Table 5), although in each case there was evidence of bimodal behavior. ^{1}H NMR spectra of the PVL again indicated that the products were catenulate. The MALDI-TOF spectra revealed several families of products including OH-terminated polymers and cyclic polymers (e.g., Figures 11 and 12; expansions are given in Figures S43–S46, SI). As for PCL, there was evidence of trans-esterification, and all observed PVL M_n values were significantly lower than the calculated values.

Table 5. The ROP of δ-VL catalyzed by **1**–**3** and **I**, **II**.

Entry	Catalyst	[VL]:[Cat]:BnOH	Conversion [a] (%) [a]	M_n (*obsd*) [b]	M_n Corrected [c]	M_n *calc* [d]	Đ [b]
1	**1**	500:1:2	93	22,160	12,630	46,570	2.38
2 [e]	**1**	500:1:2	98	29,320	16,710	49,080	1.38
3	**2**	500:1:1	83	24,390/10,910	13,900/6220	41,570	1.24/1.06
4 [e]	**2**	500:1:1	96	27,470	15,660	48,080	2.71
5	**3**	500:1:1	76	23,460	13,370	38,060	2.75
6 [e]	**3**	500:1:1	86	16,770	9560	43,070	1.90
7	**I**	500:1:1	94	10,560	6020	47,070	1.69
8[e]	**I**	500:1:1	94	24,460	13,940	47,070	2.06
9	**II**	500:1:1	98	29,400/5930	16,760/3380	49,080	1.69/1.47
10 [e]	**II**	500:1:1	97	20,440/4720	11,650/2690	48,580	1.39/1.23
11 [e]	$[2,2'\text{-}NH_2(C_6H_4)]_2$	500:1	95	15,910	9070	47,580	2.29
12 [e]	$[2,2'\text{-}(NH_2)C_6H_4]_2CH_2$	500:1	94	29,490	16,810	47,070	1.21
13 [e]	$[2,2'\text{-}(NH_2)C_6H_4]_2CH_2CH_2$	500:1	94	29,860	17,020	47,070	1.32
14 [e]	$1,2\text{-}(NH_2)(CO_2H)C_6H_4$	500:1	99	8140	4640	49,580	2.69
15 [e]	$H_2NC_6H_3\text{-}1,4\text{-}(CO_2H)_2$	500:1	13		-	-	-

[a] Determined by ^{1}H NMR spectroscopy. [b] Measured by GPC in THF relative to polystyrene standards; [c] M_n calculated after Mark–Houwink correction [44,45]: M_n corrected = 0.57 × M_n obsd; [d] Calculated from ([monomer]$_0$/[cat]$_0$) × conv (%) × monomer molecular weight (M_{VL} = 100.12) + end groups (OH used in this case). [e] Conducted in air.

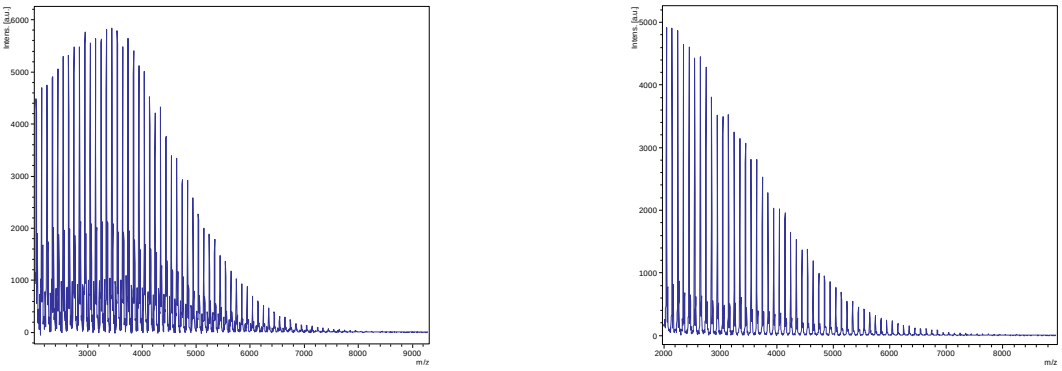

Figure 11. MALDI-ToF spectrum of PVL left using **1**: (Entry 1, Table 5); right using **2** (Entry 4, Table 5). For Entry 1, Table 5: The main families are (i) chain polymer (terminated by 2 OH) as sodium adducts [M = 17 (OH) + 1(H) + n × 100.12 (VL) + 22.99 (Na^+)], e.g., for n = 23, calc. 2343.8, obsv. 2345.8; n = 25

calc. 2544.0, obsv. 2545.9 with peaks offset by about 2 Da; (ii) cyclic polymers as the potassium adducts e.g., n = 50 calc. 5045.1, obsv. 5045.2; n = 60 calc 6046.3, obsv. 6045.2. For Entry 4, Table 5: The main families are (i) chain polymer (terminated by 2 OH) as sodium adducts [M = 17 (OH) + 1(H) + n × 100.12 (VL) + 22.99 (Na^+)] (e.g., for n = 23, calc. 2343.8, obsv. 2345.7; n = 25 calc. 2544.0, obsv. 2545.5 with peaks offset by 1.5–1.9 Da; (ii) cyclic polymers as the potassium adducts, e.g., n = 50 calc. 5045.1, obsv. 5045.2; n = 60 calc. 6046.3, obsv. 6045.5. Expansions of all the peaks highlighted above can be found in SI (Figures S41 and S42).

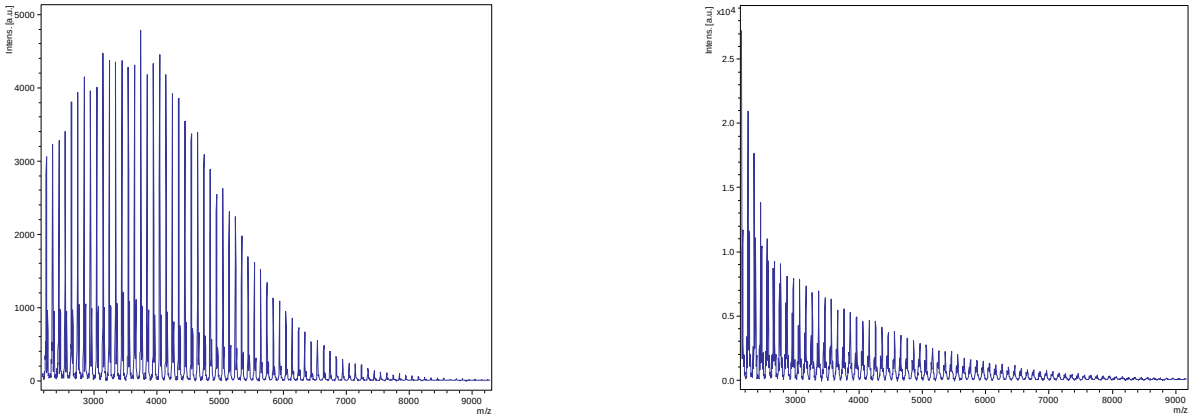

Figure 12. MALDI-ToF spectrum of PVL left using **3**: (Entry 5, Table 5); right using **II** (Entry 9, Table 5). For Entry 5, Table 5: The main families are (i) chain polymer (terminated by 2 OH) as sodium adducts [M = 17 (OH) + 1(H) + n × 100.12 (VL) + 22.99 (Na^+)], e.g., for n = 23, calc. 2343.8, obsv. 2346.4; n = 25 calc. 2544.0, obsv. 2546.1 with peaks offset by 1.6 to 2.1 Da; (ii) cyclic polymers as the potassium adducts, e.g., n = 50 calc. 5045.1, obsv. 5045.9; n = 60 calc. 6046.3, obsv. 6046.5. For Entry 9, Table 5: The main family is chain polymers (terminated by 2 OH) as sodium adducts [M = 17 (OH) + 1(H) + n × 100.12 (VL) + 22.99 (Na^+)], e.g., for n = 23, calc. 2343.8, obsv. 2345.0; n = 25 calc. 2544.0, obsv. 2544.8 with peaks offset by 0.8–1.2 Da. Expansions of all the peaks highlighted above can be found in SI (Figures S43 and S44).

Interestingly, in contrast to the ε-CL screening, when employing the dianilines for the ROP of δ-VL, high conversions were noted (see entries 11 to 13, Table 5). MALDI-ToF spectra (Figures S47–S49, SI) revealed the presence of families with OH end groups or cyclic polymers. This behavior contrasts with previous ROP studies where more robust conditions are usually needed for the ROP of δ-VL versus ε-Cl [46–50] and is inconsistent with the thermodynamic parameters for these lactones [48]. As for ε-CL, the use of 1,2-$(NH_2)(CO_2H)C_6H_4$ afforded a higher conversion than 2-$H_2NC_6H_3$-1,4-$(CO_2H)_2$ (99% vs. 13%), and in this case, anthranilic acid-derived end groups (Figure S50, SI) were assigned to a family of peaks offset by ca. 3Da; the ^{1}H NMR spectrum is given in Figure S51, SI.

TGA and DSC results (Figures S52–S55, SI) for the molybdenum catalysts employed herein indicate that at the temperature utilized for the ROP procedure, there is no degradation to other by-products.

4. Materials and Methods

All manipulations were carried out under an atmosphere of nitrogen using standard Schlenk line and cannula techniques or a conventional N_2-filled glovebox. Solvents were refluxed over the appropriate drying agents and distilled and degassed prior to use, i.e., dimethoxyethane was refluxed over Na-benzophenone/ketyl, and acetonitrile and triethylamine were refluxed over calcium hydride. Trimethylsilylchloride (TCI, Oxford, UK), 2-aminoterephthalic acid $H_2NC_6H_3$-1,4-$(CO_2H)_2$ (Thermo Fisher Scientific, Altrincham, UK), 2,2′-methylenedianiline [2,2′-$(NH_2)C_6H_4]_2CH_2$ (Enamine, Kyiv, Ukraine), 2,2′-ethylenedianiline [2,2′-$(NH_2)C_6H_4]_2CH_2CH_2$ (ChemCruz, Huissen, The Netherlands),

and anthranilic acid 1,2-$(NH_2)(CO_2H)C_6H_4$ (Sigma Aldrich, UK) were purchased from commercial sources and used directly. 2,2′-Diaminobiphenyl was prepared via reduction of the dinitro precursors using $NaBH_4$ (Sigma Aldrich, Gillingham, UK) [51]. Elemental analyses were performed at the University of Hull. FTIR spectra (nujol mulls, KBr windows) were recorded on a Nicolet Avatar 360 FT-IR spectrometer (Thermo Fisher Scientific, Altrincham, UK). ^{1}H NMR spectra were recorded at 400.2 MHz on a JEOL ECZ 400S spectrometer (JEOL, Welwyn Garden City, UK), with TMS $\delta_H = 0$ as the internal standard or residual protic solvent; chemical shifts are given in ppm (δ). Matrix Assisted Laser Desorption/Ionization-Time of Flight (MALDI-TOF) mass spectrometry was performed on a Bruker III smart beam in linear mode. MALDI-TOF mass spectra were acquired by averaging at least 100 laser shots. Molecular weight analyses were performed on a Viscotek gel permeation chromatograph (Malvern, Worcestershire, UK) equipped with two Agilent PL gel columns (5 μM mixedD, 300 × 7.5 mm; Polymer laboratories, Church Stratton, UK) and a Viscotek refractive index detector at 35 °C (Malvern Panalytical, Worcestershire, UK). Extra dry stabilized THF (Acros Organics, Loughborough, UK) was used as the eluent at a flow rate of 1.0 mL min^{-1} and polystyrene standards (Malvern Panalytical, Worcestershire, UK); 1.5 mg mL^{-1}, prepared and filtered (0.2.0 mmol L^{-1}) directly prior to injection were used for calibration. Obtained molecular weights were corrected by a Mark−Houwink factor of 0.56 (PCL) and 0.57 (PVL) [44,45]. Molecular weights were calculated from the experimental traces using the OmniSEC software (Malvern Panalytical Ltd., Malvern, UK, v11.35). For the TGA runs, data were collected on a PerkinElmer TGA 400 (Shelton, CT, USA) using Pyris^{TM} software and a rate of 10 °C per min over the 30 °C to 800 °C under N_2. Sample weights were typically between 3 and 5 mg. For DSC runs, data were collected on a PerkinElmer DSC 4000 (Shelton, CT, USA) using 5 mg of sample encapsulated with tin foil.

4.1. Synthesis of [(MoCl$_3$[2,2′-N(C$_6$H$_4$)]$_2$}{HNC$_6$H$_3$-1-(CO$_2$),4-(CO$_2$H)]·2[2,2′-NH$_2$(C$_6$H$_4$)]$_2$·3.5MeCN (1·3.5MeCN)

To Na_2MoO_4 (3.00 g, 14.6 mmol), $H_2NC_6H_3$-1,4-$(CO_2H)_2$ (2.64 g, 14.6 mmol), and [2,2′-$NH_2(C_6H_4)]_2$ (1.34 g, 7.30 mmol) in DME (150 mL) were added Et_3N (8.1 mL, 58 mmol) and Me_3SiCl (14.8 mL, 117 mmol), and the system was heated at reflux for 12 h. On cooling, the purple suspension was filtered, and the solvent was removed from the filtrate. Crystallization of the residue from MeCN (50 mL) afforded **1**·3.5MeCN as orange/red prisms. Yield 4.36 g, 41%. $C_{28}H_{18}Cl_6Mo_2N_4O_8·2(C_{12}H_{12}N_2)·1.5(C_2H_3N)$ (sample dried in-vacuo for 2 h) requires C 48.11, H 3.41, N 9.69%. Found: C 47.78, H 3.36, N 9.43%. IR: 3444bw, 2622w, 2603w, 2497w, 1715w, 1592w, 1581m, 1557m, 1397m, 1301m, 1260s, 1208w, 1171m, 1092s, 1035s, 903w, 850m, 801s, 760m, 739w, 723m, 685w, 619w, 471w, 463w, 434w. M.S. (MALDI-ToF): 1188 (M^+–2MeCN–$C_{12}H_{12}N_2$), 1111 (M^+–3MeCN–Cl–$C_{12}H_{12}N_2$), 1004 (M^+–2MeCN–2$C_{12}H_{12}N_2$), 953 (M^+–1.5MeCN–2$C_{12}H_{12}N_2$).

4.2. Synthesis of [MoCl$_2$(O$_2$CC$_6$H$_3$NHCO$_2$SiMe$_3$)(NC$_6$H$_4$CH$_2$C$_6$H$_4$NH$_2$)]·3(C$_2$H$_3$N) (2·3MeCN)

As for **1**, but using Na_2MoO_4 (3.00 g, 14.6 mmol), $H_2NC_6H_3$-1,4-$(CO_2H)_2$ (2.64 g, 14.6 mmol), [2,2′-$(NH_2)C_6H_4]_2CH_2$ (1.45 g, 7.31 mmol), Et_3N (8.1 mL, 58 mmol), and Me_3SiCl (14.8 mL, 117 mmol) in DME (150 mL) affording **2**·3MeCN as red crystals. Yield 3.88 g, 36%. $C_{24}H_{25}Cl_2MoN_3O_4Si·2(C_2H_3N)$ (sample dried in vacuo for 1 h) requires C 48.28, H 4.49, N 10.06%. Found: C 47.79, H 4.31, N 9.91%. IR: 3501w, 3446w, 3385w, 1692m, 1624m, 1591m, 1552m, 1309s, 1260s, 1239s, 1170m, 1155m, 1089m, 1020m, 918m, 891m, 850m, 796m, 752s, 722s, 679w, 657w, 623w. M.S. (MALDI-ToF): 499 (MH^+–MeCN–$C_{13}H_{14}N_2$).

4.3. Synthesis of [MoCl$_3${1,2-(NH)(CO$_2$)C$_6$H$_4$}{NC$_6$H$_4$CH$_2$CH$_2$C$_6$H$_4$NH$_3$}]·MeCN (3·MeCN)

To Na_2MoO_4 (3.00 g, 14.6 mmol), 1,2-$(NH_2)(CO_2H)C_6H_4$ (2.00 g, 14.6 mmol), and [2,2′-$(NH_2)C_6H_4]_2CH_2CH_2$ (1.55 g, 7.30 mmol) in DME (150 mL) were added Et_3N (8.1 mL, 58 mmol) and Me_3SiCl (14.8 mL, 117 mmol), and the system was heated at reflux for 12 h. On cooling, the purple suspension was filtered, and the solvent was removed from the

filtrate. Crystallization of the residue from MeCN (50 mL) afforded **3**·MeCN as purple crystals. Yield 2.32 g, 27%. $C_{21}H_{20}Cl_3MoN_3O_2$ (sample dried in vacuo for 1 h) requires C 45.97, H 3.67, N 7.66%. Found: C 45.33, H 3.52, N 7.37%. IR: 3452w, 3348w, 2358w, 2250w, 2139w, 1939w, 1914w, 1667w, 1614m, 1585m, 1562m, 1536m, 1397s, 1331m, 1260m, 1171s, 1072m, 1036s, 941m, 906m, 851m, 807s, 763m, 723m, 663w. M.S. (MALDI-ToF): 452 (M^+–anthranilic acid).

4.4. ROP of ε-Caprolactone (ε-CL)

The pre-catalyst (0.010 mmol) was added to a Schlenk tube in the glovebox at room temperature. The appropriate equivalent of BnOH (from a pre-prepared stock solution of 1 mmol BnOH in 100 mL toluene) was added, and the system was stirred for 5 min and then the solvent was removed in vacuo. The appropriate amount of ε-CL was added, and the reaction mixture was then placed into a sand bath pre-heated at 130 °C and heated for the prescribed time (24 h) under either N_2 or air. The polymerization mixture was quenched on addition of an excess of glacial acetic acid (0.2 mL) in methanol (50 mL). The resultant polymer was then collected on filter paper and was dried in vacuo. GPC (in THF) was used to determine molecular weights (M_n and PDI) of the polymer products.

4.5. X-ray Crystallography

In all cases, crystals suitable for an X-ray diffraction study were grown from a saturated MeCN solution at 0 °C. Diffraction data for **1**·2[2,2′-$NH_2(C_6H_4)]_2$·3.5MeCN and **2**·3MeCN were collected on pixel array detector-equipped Rigaku diffractometers using a rotating anode X-ray source, while that for **3**·MeCN was collected on a Bruker SMART 1K CCD (Bruker AXS, Madison, WI, USA) diffractometer equipped with a sealed-tube X-ray source [52]. Data were corrected for absorption, polarization, and Lp effects. All of the structures were solved and refined routinely [53–56]. H atoms were included in a riding model except the N*H* hydrogens in **2**·3MeCN and **3**·MeCN, where the coordinates were refined with mild distance restraints. U_{iso}(H) was set to 120% of that of the carrier atoms except for O*H*, NH_3, and CH_3 (150%). Further details are presented in Table 6. CCDC 2,286,024–2,286,026 contain the supplementary crystallographic data for this paper. These data can be obtained free of charge from The Cambridge Crystallographic Data Centre via www.ccdc.cam.ac.uk/structures (accessed 20 March 2024).

Table 6. Crystallographic data for **1**·2$C_{12}H_{12}N_2$·3.5MeCN, **2**·3MeCN, and **3**·MeCN.

Compound	**1·2$C_{12}H_{12}N_2$·3.5MeCN**	**2·3MeCN**	**3·MeCN**
CCDC No.	2,286,024	2,286,025	2,286,026
Formula	$C_{28}H_{18}Cl_6Mo_2N_4O_8$·2($C_{12}H_{12}N_2$)·3.5($C_2H_3N$)	$C_{24}H_{25}Cl_2MoN_3O_4Si$·3($C_2H_3N$)	$C_{21}H_{20}Cl_3MoN_3O_2$·(C_2H_3N)
Formula weight	1455.20	737.56	589.74
Crystal system	Monoclinic	Monoclinic	Monoclinic
Space group	*Cc*	$P2_1/n$	$P2_1/c$
Unit cell dimensions			
a (Å)	12.2500(2)	15.57139(19)	17.9901(13)
b (Å)	31.4061(7)	13.33765(14)	16.5331(12)
c (Å)	16.2619(2)	17.8684(2)	18.5902(13)
β (°)	97.3910(13)	110.7234(14)	114.058(2)
V (Å^3)	6204.37(19)	3470.91(7)	5049.0(6)
Z	4	4	8
Temperature (K)	100(2)	100(2)	160(2)
Wavelength (Å)	1.54178	0.71073	0.71073
Calculated density (g.cm^{-3})	1.558	1.411	1.552
Absorption coefficient (mm^{-1})	6.22	0.61	0.87

Table 6. *Cont.*

Compound	**1**·2$C_{12}H_{12}N_2$·3.5MeCN	**2**·3MeCN	**3**·MeCN
Transmission factors (min./max.)	0.045 and 0.143	0.761 and 1.000	0.674 and 0.862
Crystal size (mm^3)	0.04 × 0.04 × 0.02	0.20 × 0.14 × 0.01	0.20 × 0.20 × 0.14
θ(max) (°)	75.7	33.6	28.5
Reflections measured	20,721	143,190	30,725
Unique reflections	8359	12,893	11,549
R_{int}	0.052	0.035	0.046
Reflections with $F^2 > 2\sigma(F^2)$	7358	11,128	7877
Number of parameters	798	412	621
R_1 [$F^2 > 2\sigma(F^2)$]	0.058	0.031	0.041
wR_2 (all data)	0.144	0.072	0.094
GOOF, *S*	1.03	1.05	0.99
Largest difference peak and hole (e $Å^{-3}$)	1.67 and −0.36	0.87 and −0.80	0.51 and −0.96

5. Conclusions

In conclusion, the use of dianilines with $(CH_2)_n$ bridges where n = 0 to 2, when reacted with sodium molybdate in the presence of Et_3N/Me_3SiCL in 1,2-dimethoxyethane in combination with the acid-functionalized acids anthranilic acid or 2-aminoterephthalic acid, leads to the isolation of unusual H-bonded arrays. Relatively few molybdenum-based ROP catalysts have been reported in the literature. The systems reported herein are active as catalysts for the ROP of ε-caprolactone when employed as melts under either air or N_2. The products are of relatively high molecular weight (10,420–56,510 Da) and generally with broad Đ (1.12–3.08). A number of families were evident in the MALDI-ToF mass spectra with polymers present assigned to those terminated with OH, BnO (PCL only), as well as cyclic polymers. The parent dianilines were found to be capable of the ROP of δ-VL, but not ε-CL. The acids anthranilic acid or 2-aminoterephthalic acid were capable of the ROP of both cyclic esters; in terms of conversion, anthranilic acid outperformed 2-aminoterephthalic acid the best. All of these systems are thought to benefit from the presence of H-bonding, which has been shown in other studies to boost ROP performance [31–36].

Supplementary Materials: The following supporting information can be downloaded at: https://www.mdpi.com/article/10.3390/catal14030214/s1, Figure S1. IR spectrum of **1**; Figure S2. Different views of the molecular structures of **1**; Figure S3. MALDI-ToF spectrum of **1**; Figure S4. ^{1}H NMR spectrum of aromatic region of **1**; Figure S5. IR spectrum of **2**; Figure S6. Different views of the molecular structures of **2**; Figure S7. MALDI-ToF spectrum of **2**; Figure S8. IR spectrum of **3**; Figure S9. Different views of the molecular structures of **3**; Figure S10. MALDI-ToF spectrum of **3**; Figures S11–S14. Selected ^{1}H NMR spectra for %conversion measurements; Figures S15–S21. Selected gpc traces; Figures S22–S25. Expansions of MALDI-ToF spectra of PCL obtained from **1**–**3**; Figure S26. MALDI-ToF spectrum of PCL obtained using anthranilic acid; Figure S27. ^{1}H spectrum of PCL obtained using anthranilic acid; Figures S28–S35. Selected ^{1}H NMR spectra for %conversion measurements; Figures S36–S42. Selected gpc traces; Figures S43–S46. Expansions of MALDI-ToF spectra of PCL obtained from **1**–**3**; Figure S47. MALDI-ToF of PVL using [2,2′-$NH_2(C_6H_4)]_2$ (run 11, Table 5); Figure S48. MALDI-ToF of PVL using $[2,2'\text{-}(NH_2)C_6H_4]_2CH_2$ (run 12, Table 5); Figure S49. MALDI-ToF of PVL using $[2,2'\text{-}(NH_2)C_6H_4]_2CH_2CH_2$ (run 13, Table 5); Figure S50. MALDI-ToF spectrum of PVL obtained using anthranilic acid; Figure S51. ^{1}H NMR spectrum for PVL using anthranilic acid; Figure S52. TGA for **2**·3MeCN; Figure S53. DSC for **2**·3MeCN; Figure S54. TGA for **II**; Figure S55. DSC for **II**.

Author Contributions: W.C.: Investigation, Writing—review and editing. M.R.J.E.: Investigation, Writing—review and editing. C.R.: Conceptualization, Writing—original draft, Writing—review and editing. All authors have read and agreed to the published version of the manuscript.

Funding: This research was funded by UKRI Creative Circular Plastic grant (EP/S025537/1).

Data Availability Statement: Data is available upon requested.

Acknowledgments: The EPSRC National Crystallographic Service Centre at Southampton University is thanked for data collection of **1**·2[2,2′-$NH_2(C_6H_4)]_2$·3.5MeCN and **2**·3MeCN.

Conflicts of Interest: There are no conflicts of interest to declare.

References

1. Schrock, R.R.; Hoveyda, A.H. Molybdenum and Tungsten Imido Alkylidene Complexes as Efficient Olefin-Metathesis Catalysts. *Angew. Chem. Int. Ed.* **2003**, *42*, 4592–4633. [CrossRef] [PubMed]
2. Gibson, V.C.; Redshaw, C.; Clegg, W.; Elsegood, M.R.J. Synthesis and characterisation of molybdenum complexes bearing highly functionalised imido substituents. *Dalton Trans.* **1997**, 3207–3212. [CrossRef]
3. Redshaw, C.; Gibson, V.C.; Clegg, W.; Edwards, A.J.; Miles, B. Pentamethylcyclopentadienyl tungsten complexes containing imido, hydrazido and amino acid derived N-O chelate ligands. *Dalton Trans.* **1997**, 3343–3347. [CrossRef]
4. Gibson, V.C.; Redshaw, C.; Clegg, W.; Elsegood, M.R.J. Carboxylate versus imidobenzoate bonding for anthranilic acid derivatives. Crystals structures of [W(η-Cp*)Cl_3(η^2-$O_2CC_6H_4NH_2$-2)] and [ReCl(OEt)$(PPh_3)_2(NC_6H_4CO_2)$]. *Inorg. Chem. Commun.* **2001**, *4*, 95–99. [CrossRef]
5. Humphrey, S.M.; Redshaw, C.; Holmes, K.E.; Elsegood, M.R.J. Acid/amide bonding for anthranilic acid derivatives: Crystal structures of W(X)$Cl_3(HO_2CC_6H_4NH$-2) (X = O, NPh). *Inorg. Chim. Acta* **2005**, *358*, 222–226. [CrossRef]
6. Gibson, V.C.; Redshaw, C.; Clegg, W.; Elsegood, M.R.J.; Siemeling, U.; Turk, T. Synthesis and X-ray crystal structures of hydridotris(3,5-dimethylpyrazolyl)borate (Tp′) molybdenum(VI) bis(imido) complexes. *Polyhedron* **2004**, *23*, 189–194. [CrossRef]
7. Gibson, V.C.; Redshaw, C.; Clegg, W.; Elsegood, M.R.J. Supramolecular metallocalixarene chemistry: Linking metallocalixarenes through imido bridges. *Chem. Commun.* **1998**, 1969–1970. [CrossRef]
8. Gibson, V.C.; Redshaw, C.; Clegg, W.; Elsegood, M.R.J.; Siemeling, U.; Türk, T. Bridged bis(imido)molybdenum complexes: Isolobal analogues of *ansa*-zirconocenes and bizirconocenes. *J. Chem. Soc. Dalton Trans.* **1996**, 4513–4515. [CrossRef]
9. Siemeling, U.; Tűrk, T.; Schoeller, W.W.; Redshaw, C.; Gibson, V.C. Benefits of the chelate effect: Preparation of an unsymmetrical *ansa*-bis(imido)molybdenum complex containing a seven-membered chelate ring. *Inorg. Chem.* **1998**, *37*, 4738–4739. [CrossRef]
10. Redshaw, C.; Gibson, V.C.; Elsegood, M.R.J.; Clegg, W. New coordination modes at molybdenum for 2-diphenylphosphinoaniline derived ligands. *Chem. Commun.* **2007**, 1951–1953. [CrossRef]
11. Yang, W.; Zhao, Q.-K.; Redshaw, C.; Elsegood, M.R.J. Molybdenum complexes derived from the oxydianiline [$(2\text{-}NH_2C_6H_4)_2$O]: Synthesis, characterization and ε-caprolactone ROP capability. *Dalton Trans.* **2015**, *44*, 13133–13140. [CrossRef]
12. Kretzschmar, E.A.; Kipke, J.; Sundermeyer, J. The first chiral diimido chelate complexes of molybdenum and tungsten: Transition metal diimido complexes on the way to asymmetric catalysis. *Chem. Commun.* **1999**, 2381–2382. [CrossRef]
13. Singh, N.; Ogunseitan, O.A.; Wong, M.H.; Tang, Y. Sustainable materials alternative to petrochemical plastics pollution: A review analysis. *Sustain. Horiz.* **2022**, *2*, 100016. [CrossRef]
14. Keefe, B.J.; Hillmeyer, M.A.; Tolman, W.B. Polymerization of lactide and related cyclic esters by discrete metal complexes. *J. Chem. Soc. Dalton Trans.* **2001**, 2215–2224. [CrossRef]
15. Dechy-Cabaret, O.; Martin-Vaca, B.; Bourissou, D. Controlled Ring-Opening Polymerization of Lactide and Glycolide. *Chem. Rev.* **2004**, *104*, 6147–6176. [CrossRef] [PubMed]
16. Labet, M.; Thielemans, W. Synthesis of polycaprolactone: A review. *Chem. Soc. Rev.* **2009**, *38*, 3484–3504. [CrossRef] [PubMed]
17. Thomas, C.M. Stereocontrolled ring-opening polymerization of cyclic esters: Synthesis of new polyester microstructures. *Chem. Soc. Rev.* **2010**, *39*, 165–173. [CrossRef] [PubMed]
18. Arbaoui, A.; Redshaw, C. Metal catalysts for ε-caprolactone polymerisation. *Polym. Chem.* **2010**, *1*, 801–826. [CrossRef]
19. Dove, A.P. Organic Catalysis for Ring Opening Polymerization. *ACS Macro Lett.* **2012**, *1*, 1409–1412. [CrossRef]
20. Sarazin, Y.; Carpentier, J.-F. Discrete Cationic Complexes for Ring-Opening Polymerization Catalysis of Cyclic Esters and Epoxides. *Chem. Rev.* **2015**, *115*, 3564–3614. [CrossRef]
21. Gao, J.; Zhu, D.; Zhang, W.; Solan, G.A.; Ma, Y.; Sun, W.-H. Recent progress in the application of group 1, 2 & 13 metal complexes as catalysts for the ring opening polymerization of cyclic esters. *Inorg. Chem. Front.* **2019**, *6*, 2619–2652.
22. Nifant'ev, I.; Ivchenko, P. Coordination Ring-Opening Polymerization of Cyclic Esters: A Critical Overview of DFT Modeling and Visualization of the Reaction Mechanisms. *Molecules* **2019**, *24*, 4117. [CrossRef]
23. Tazekas, E.; Lowy, P.A.; Rahman, M.A.; Lykkeberg, A.; Zhou, Y.; Chambenahalli, R.; Garden, J.A. Main group metal polymerisation catalysts. *Chem. Soc. Rev* **2022**, *51*, 8793–8814. [CrossRef]
24. Naz, F.; Abdur, R.M.; Mumtaz, F.; Elkadi, M.; Verpoort, F. Advances in cyclic ester ring-opening polymerization using heterogeneous catalysts. *Appl. Organomet. Chem.* **2023**, *37*, e7296. [CrossRef]
25. Wang, Y.; Wang. X.; Zhang, W.; Sun, W.-H. Progress of Ring Opening Polymerization of Cyclic Esters Catalyzed by Iron Compounds. *Organometallics* **2023**, *42*, 1680–1692. [CrossRef]
26. Báez, J.E.; Martˇnez-Richa, A. Synthesis and characterization of poly(ε-caprolactone) and copolyesters by catalysis with molybdenum compounds: Polymers with acid-functional asymmetric telechelic architecture. *Polymer* **2005**, *46*, 12118. [CrossRef]
27. Maruta, Y.; Abiko, A. Bis(salicylaldehydato)dioxomolybdenum complexes: Catalysis for ring-opening polymerization. *Polym. Bull.* **2014**, *71*, 1433. [CrossRef]

28. Al-Khafaji, Y.; Prior, T.J.; Elsegood, M.R.J.; Redshaw, C. Molybdenum(VI) imido complexes derived from chelating phenols: Synthesis, characterization and ε-caprolactone ROP capability. *Catalysts* **2015**, *5*, 1928–1947. [CrossRef]
29. Sun, Z.; Zhao, Y.; Prior, T.J.; Elsegood, M.R.J.; Wang, K.; Xing, T.; Redshaw, C. Mono-oxo molybdenum(VI) and tungsten(VI) complexes bearing chelating aryloxides: Synthesis, structure and ring opening polymerization of cyclic esters. *Dalton Trans.* **2019**, *48*, 1454–1466. [CrossRef] [PubMed]
30. Xing, T.; Elsegood, M.R.J.; Dale, S.H.; Redshaw, C. Pentamethylcyclopentadienyl molybdenum(V) complexes derived from iodoanilines: Synthesis, structure, and ROP of ε-caprolactone. *Catalysts* **2021**, *11*, 1554. [CrossRef]
31. Xu, S.; Zhu, H.; Li, Z.; Wei, F.; Gao, Y.; Xu, J.; Wang, H.; Liu, J.; Guo, T.; Guo, K. Tuning the H-bond donicity boosts carboxylic acid efficiency in ring-opening polymerization. *Eur. Polym. J.* **2019**, *112*, 799–808. [CrossRef]
32. Jehanno, C.; Mezzasalma, L.; Sardon, H.; Ruipérez, F.; Coulembier, O.; Taton, D. Benzoic Acid as an Efficient Organocatalyst for the Statistical Ring Opening Copolymerization of ε-Caprolactone and *L*-Lactide: A Computational Investigation. *Macromolecules* **2019**, *52*, 9238–9247. [CrossRef]
33. Liu, J.; Chen, C.; Li, Z.; Wu, W.; Zhi, X.; Zhang, Q.; Wu, H.; Wang, X.; Cui, S.; Guo, K. A squaramide and tertiary amine: An excellent hydrogen-bonding pair organocatalyst for living polymerization. *Polym. Chem.* **2015**, *6*, 3754–3757. [CrossRef]
34. Liu, J.; Xu, J.; Li, Z.; Xu, S.; Wang, X.; Wang, H.; Guo, T.; Gao, Y.; Zhang, L.; Guo, K. Squaramide and amine binary H-bond organocatalysis in polymerizations of cyclic carbonates, lactones, and lactides. *Polym. Chem.* **2017**, *8*, 7054–7068. [CrossRef]
35. Du, F.; Zheng, Y.; Yuan, W.; Shan, G.; Bao, Y.; Jie, S.; Pan, P. Solvent-Free Ring-Opening Polymerization of Lactones with Hydrogen Bonding Bisurea Catalyst. *J. Polym. Sci. Part A Polym. Chem.* **2019**, *57*, 90–100. [CrossRef]
36. Jain, I.; Malik, P. Advances in urea and thiourea catalyzed ring opening polymerization: A brief overview. *Eur. Polym. J.* **2020**, *133*, 109791. [CrossRef]
37. Printz, G.; Ryzhakov, D.; Gourlaouen, C.; Jacques, B.; Messaoudi, S.; Dumas, F.; Le Bideau, F.; Dagorne, S. First Use of Thiosquaramides as Polymerization Catalysts: Controlled ROP of Lactide Implicating Key Secondary Interactions for Optimal Performance. *ChemCatChem* **2024**, *16*, e202301207. [CrossRef]
38. Kazakov, O.I.; Datta, P.P.; Isajani, M.; Kiesewetter, E.T.; Kiesewetter, M.K. Cooperative Hydrogen-Bond Pairing in Organocatalytic Ring Opening Polymerization. *Macromolecules* **2014**, *47*, 7463–7468. [CrossRef] [PubMed]
39. Spink, S.S.; Kazakov, O.I.; Kiesewetter, E.T.; Kiesewetter, M.K. Rate Accelerated Organocatalytic Ring-Opening Polymerization of *L*-Lactide via the Application of a Bis(thiourea) H-bond Donating Cocatalyst. *Macromolecules* **2015**, *48*, 6127–6131. [CrossRef] [PubMed]
40. Etter, M.C.; MacDonald, J.C.; Bernstein, J. Graph-set analysis of hydrogen-bond patterns in organic crystals. *Acta Cryst.* **1990**, *B46*, 256–262. [CrossRef] [PubMed]
41. Bernstein, J.; Davis, R.E.; Shimoni, L.; Chang, N.-L. Patterns in Hydrogen Bonding: Functionality and Graph Set Analysis in Crystals. *Angew Chem. Int. Ed. Engl.* **1995**, *34*, 1555–1573. [CrossRef]
42. Groom, C.R.; Bruno, I.J.; Lightfoot, M.P.; Ward, S.C. The Cambridge Structural Database. *Acta Cryst.* **2016**, *B72*, 171–179. [CrossRef]
43. Basenko, S.V.; Soldatenko, A.S.; Vashchenko, A.V.; Smimov, V.I. Silacyclophanones 3*. Cyclic organosilicon esters of *ortho*-phthalic acids. *Chem. Heterocycl. Compd.* **2019**, *55*, 1139. [CrossRef]
44. Shah, S.A.A.; Dorn, H.; Gindl, J.; Noltemeye, M.; Schmidt, H.-G.; Roesky, H.W. Synthesis and structural characterization of sulfonates, phosphinates and carboxylates of organometallic Group 4 metal fluorides. *J. Organomet. Chem.* **1998**, *550*, 1–6. [CrossRef]
45. Basenko, S.V.; Soldatenko, A.S.; Vashchenko, O.V.; Smirnov, V.I. Silacyclophanones 2*. Cyclic organosilicon esters of terephthalic acid. Chem. *Heterocycl. Compd.* **2018**, *54*, 826–828. [CrossRef]
46. Huang, C.-H.; Wang, F.-C.; Ko, B.-T.; Yu, T.-L.; Lin, C.-C. Ring-Opening Polymerization of ε-Caprolactone and L-Lactide Using Aluminum Thiolates as Initiator. *Macromolecules* **2001**, *34*, 356–361. [CrossRef]
47. Save, M.; Schappacher, M.; Soum, A. Controlled Ring-Opening Polymerization of Lactones and Lactides Initiated by Lanthanum Isopropoxide, 1. General Aspects and Kinetics. *Macromol. Chem. Phys.* **2002**, *203*, 889–899. [CrossRef]
48. Al-Khafaji, Y.F.; Elsegood, M.R.J.; Frese, J.W.A.; Redshaw, C. Ring opening polymerization of lactides and lactones by multimetallic alkyl zinc complexes derived from the acids $Ph_2C(X)CO_2H$ (X = OH, NH_2). *RSC Adv.* **2017**, *7*, 4510–4517. [CrossRef]
49. Wang, X.; Zhao, K.-Q.; Al-Khafaji, Y.; Mo, S.; Prior, T.J.; Elsegood, M.R.J.; Redshaw, C. Organoaluminium complexes derived from anilines or Schiff bases for the ring-opening polymerization of ε-caprolactone, δ-valerolactone and *rac*-lactide. *Eur. J. Inorg. Chem.* **2017**, *2017*, 1951–1965. [CrossRef]
50. *Handbook of Ring Opening Polymerization*; Dubois, P.; Coulembier, O.; Raquez, J.-M. (Eds.) Wiley-VCH: Weinheim, Germany, 2009. [CrossRef]
51. Aikawa, K.; Mikami, K. Dual chirality control of palladium(II) complexes bearing *Tropos* biphenyl diamine ligands. *Chem. Commun.* **2005**, 5799–5801. [CrossRef] [PubMed]
52. *APEX 2 & SAINT Software for CCD Diffractometers*; Bruker AXS Inc.: Madison, WI, USA, 2006.
53. *CrysAlisPRO Software, Oxford Rigaku Diffraction*; Rigaku Corporation: Wrocław, Poland, 2021 & 2023.
54. Sheldrick, G.M. Crystal structure refinement with SHELXL. *Acta Cryst.* **2015**, *C71*, 3–8. [CrossRef]

55. Sheldrick, G.M. *SHELXT*—Integrated space-group and crystal-structure determination. *Acta Cryst.* **2015**, *A71*, 3–8. [CrossRef] [PubMed]
56. Palatinus, L.; Chapuis, G. SUPERFLIP—A computer program for the solution of crystal structures by charge flipping in arbitrary dimensions. *J. Appl. Cryst.* **2007**, *40*, 786–790. [CrossRef]